Published in final edited form as:
*J Biomed Mater Res*. 2001 May ; 55(2): 242–253.

# Bone tissue engineering in a rotating bioreactor using a microcarrier matrix system

**E. A. Botchwey**[1,2], **S. R. Pollack**[2,3], **E. M. Levine**[4], and **C. T. Laurencin**[1,5]

[1]Center for Advanced Biomaterials and Tissue Engineering, Department of Chemical Engineering, Drexel University, 3141 Chestnut Street, Philadelphia, Pennsylvania 19104

[2]Department of Bioengineering, University of Pennsylvania, Philadelphia, Pennsylvania

[3]Department of Orthopedic Surgery, University of Pennsylvania, Philadelphia, Pennsylvania

[4]The Wistar Institute, Philadelphia, Pennsylvania

[5]Department of Orthopaedic Surgery, MCP-Hahnemann School of Medicine, Philadelphia, Pennsylvania

## Abstract

A novel approach was utilized to grow *in vitro* mineralized bone tissue using lighter-than-water, polymeric scaffolds in a high aspect ratio rotating bioreactor. We have adapted polymer microencapsulation methods for the formation of hollow, lighter-than-water microcarriers of degradable poly(lactic-*co*-glycolic acid). Scaffolds were fabricated by sintering together lighter-than-water microcarriers from 500 to 860 μm in diameter to create a fully interconnected, three-dimensional network with an average pore size of 187 μm and aggregate density of 0.65 g/mL. Motion in the rotating bioreactor was characterized by numerical simulation and by direct measurement using an *in situ* particle tracking system. Scaffold constructs established a near circular trajectory in the fluid medium with a terminal velocity of 98 mm/s while avoiding collision with the bioreactor wall. Preliminary cell culture studies on these scaffolds show that osteoblast-like cells readily attached to microcarrier scaffolds using controlled seeding conditions with an average cell density of $6.5 \times 10^4$ cells/cm$^2$. The maximum shear stress imparted to attached cells was estimated to be 3.9 dynes/cm$^2$. In addition, cells cultured *in vitro* on these lighter-than-water scaffolds retained their osteoblastic phenotype and showed significant increases in alkaline phosphatase expression and alizarin red staining by day 7 as compared with statically cultured controls.

### Keywords

tissue engineering; bone; poly(lactide-*co*-glycolide); bioreactor; scaffold

## INTRODUCTION

In 1993, Langer and Vacanti et al.[1,2] estimated the number of bone repair procedures performed in the United States at over 800,000 per year. Today, skeletal reconstruction has become an increasingly common and important procedure for the orthopedic surgeon. Conventional approaches in bone repair have involved biological grafts such as autogenous bone or autografts, allogenic bone or allografts and xenografts.[3] Currently, autograft is the



Correspondence to: C. T. Laurencin; Laurencin@drexel.edu.

preferred biological graft most often used in the clinical setting, having success rates as high as 80–90% and no risk of immune rejection or disease transfer.[4] However, the limited availability of autografts and risks of donor site morbidity have fueled great interest in the development of alternative approaches to bone repair.

Numerous tissue-engineering solutions have been proposed to address the need for new bone-graft substitutes. One potentially successful repair solution seeks to mimic the success of autografts by removing cells from the patient by biopsy and growing sufficient quantities of mineralized tissue *in vitro* on implantable, three-dimensional (3-D) scaffolds for use as a functionally equivalent autogenous bone tissue. In this way, an ideal bony repair environment is created by reproducing the intrinsic properties of autogenous bone material, which include the following: 1. a porous, 3-D architecture allowing osteoblast, osteoprogenitor cell migration and graft revascularization, 2. the ability to be incorporated into the surrounding host bone and to continue the normal bone remodeling processes, and 3. the delivery of bone-forming cells and osteogenic growth factors to accelerate healing and differentiation of local osteoprogenitor cells.[3,5]

Researchers in our laboratory and others have investigated biodegradable scaffolds for *in vitro* bone engineering, which possess a suitable 3-D environment for the cell function together with the capacity for gradual resorption and replacement by host bone tissue.[6–18] This 3-D matrix milieu provides the necessary microenvironment for cell–cell and cell–matrix interaction, and is sufficient for the production of limited amounts of mineralized bone matrix in static culture. To demonstrate clinical feasibility of tissue-engineered bone and to sufficiently match the intrinsic properties of autogenous bone-graft material, rapid mineralization of osteoid tissue grown *in vitro* must be achieved. Unfortunately, nonhomogeneous cell seeding confines cell density to the near surface of the scaffold and mineralized tissue formation is limited by inadequate diffusion of oxygen, nutrients, and waste. Using porous poly(lactide-*co*-glycolide) (PLAGA) foams with pore sizes ranging from 150 to 710 μm., Ishaug-Riley et al.[13] have observed a limit to osseous tissue ingrowth and mineralization in a static culture environment of about 200 μm. Although it is possible that structures with larger pores would facilitate greater diffusion, important cell–cell interactions and scaffold mechanical integrity might be compromised.

To circumvent some of the limitations associated with static 3-D culture, we have developed novel 3-D culturing methods for the growth of mineralized tissues *in vitro* using a rotating bioreactor. Several groups have reported on the formation of 3-D assemblies of various cell types in the rotating bioreactor.[14,19–25] It has been shown that osteoblast-like MC3T3 cells formed cell aggregates when grown on nondegradable microspheres, and these cells produced collagen fibrils in the matrix between microspheres.[20] Also, rat stromal cells cultured for 2 weeks on cytodex-3 beads formed aggregates and began to synthesize mineralized matrix, showing elevated expression of type I collagen and osteopontin.[22] However, we have reported in a previous study[21] that when such microspheres with greater density than the surrounding medium are placed in a rotating bioreactor, centrifugal force induces heavier-than-water microspheres to move outward and collide with the bioreactor wall. These collisions have been shown to induce cell damage and are a confounding variable in tissue engineering. Conversely, when lighter-than-water microspheres made from nondegradable polystyrene are placed in the rotating bioreactor, they gradually move toward the center of the bioreactor and completely avoid collisions with the bioreactor wall.[21] We hypothesized that the combination of three-dimensionality and fluid flow, in the absence of confounding wall collisions, would increase the rate and extent of mineralized tissue formation in the rotating bioreactor. Therefore, we fabricated lighter-than-water, biodegradable microcarriers and novel microcarrier scaffolds, which are ideal for testing this hypothesis in the rotating bioreactor. Our hypothesis is that these constructs will exhibit

controllable and quantifiable motion in a bioreactor environment which enhances fluid transport throughout the scaffold, and that these scaffolds support osteoblast cell attachment, growth, and phenotypic expression over short-term culture, ultimately resulting in enhanced synthesis of mineralized bone graft quality tissue. This report describes the first stage of this effort and presents the scaffold materials synthesis methods and 7-day culture results using SaOS-2 bone cells.

## MATERIALS AND METHODS

### Buoyant microcarrier fabrication

We have adapted conventional microsphere fabrication techniques for the formation of hollow, lighter-than-water microcarriers of bioerodible poly(D,L-lactic-*co*-glycolide) co-polymer.[26–31] Briefly, a 25% w/v polymer solution of 50:50 PLAGA ($M_w$ ~ 30,000) was dissolved in methylene chloride, and poured slowly into a 1000-mL beaker containing 0.1% poly(vinyl alcohol) (PVA) (lot no. 413322, MW 25,000; Poly-sciences, Warrington, PA). The solution was stirred continuously (model BDC1850; Caframo, Wiarton, Ontario, Canada) at 1000 rpm for 4–6 h to allow for solvent evaporation. Buoyant microcarriers were harvested by vacuum filtration (54 mm; Whatman, Clifton, NJ), washed with deionized water, and lyophilized (Lyph-lock 12; Labconco Corp., Kansas City, MO) for 24 h. Size distribution was determined by mechanically sifting the microcarriers using a series of stainless steel sieves with selected mesh sizes. Microcarriers were freeze fractured and analyzed with scanning electron microscopy (SEM) to confirm that the carriers were indeed hollow. *In vitro* buoyancy was verified over 7 days by immersion inside a watertight container maintained at 37°C in an oscillating (60 opm) water bath.

### Scaffold fabrication and characterization

Microcapsules of a selected size range and weight were poured into a stainless steel mold and heated in an oven (Precision Gravity Convection Incubator; Chicago, IL) for 1 h at 60°C, several degrees above the glass transition temperature for the PLAGA 50:50 ($T_g$ = 45°–50°C). Microcarriers bonded to each other while maintaining their hollow, spherical geometry. Scaffolds used for bioreactor culture were exposed to ultraviolet irradiation for 30 min on each side in an effort to minimize bacterial contamination. Microcarrier scaffolds were characterized using a low field emission scanning electron microscope (JEOL 6300; Tokyo, Japan). For SEM, specimens were coated with gold and examined for pore inter-connectivity, degree of microcarrier bonding, and deformation of microcarriers. The porosity of the structure was measured by porosimetry using the Micromeritics (Norcross, GA) Autopore III porosimeter. Specifically, cylindrical polymer scaffolds, 4 mm in diameter and approximately 2.5 mm in length were placed in a 5-mL penetrometer, subjected to a vacuum of 50 μm Hg, and infused with mercury. Porosity is determined by measuring the volume of the mercury infused. In addition to an overall percentage of porosity for the polymer scaffold, porosimetry will also give an approximate distribution of pore sizes within the polymer scaffold, allowing for more accurate characterization of the scaffold geometry.

### Numerical model simulation and particle motion analysis

In a previous study,[21] we solved the equations of motion governing microcarrier motion in the rotating bioreactor. For the particle position ($x$, $y$) and velocity ($v_x$, $v_y$), microcapsule motion relative to the rotating fluid is governed by the following equations:

$$
\begin{aligned}
\frac{dx}{dt} &= v_x \\
\frac{dv_x}{dt} &= -\frac{1}{\rho_{\text{part}} \cdot V_{\text{part}}} \begin{bmatrix} p \cdot S \cdot C_d \cdot v_x + \left(\rho_{\text{part}} - \rho_{\text{fluid}}\right) \\ \cdot V_{\text{part}} \cdot \omega^2 \cdot x + 2 \cdot \left(\rho_{\text{part}} - \rho_{\text{fluid}}\right) \\ \cdot V_{\text{part}} \cdot \omega \cdot x - \left(\rho_{\text{part}} - \rho_{\text{fluid}}\right) \\ \cdot V_{\text{part}} \cdot g \cdot \sin(\omega t) \end{bmatrix} \\
\frac{dy}{dt} &= v_y \\
\frac{dv_y}{dt} &= -\frac{1}{\rho_{\text{part}} \cdot V_{\text{part}}} \begin{bmatrix} p \cdot S \cdot C_d \cdot v_y + \left(\rho_{\text{part}} - \rho_{\text{fluid}}\right) \\ \cdot V_{\text{part}} \cdot \omega^2 \cdot y - 2 \cdot \left(\rho_{\text{part}} - \rho_{\text{fluid}}\right) \\ \cdot V_{\text{part}} \cdot \omega \cdot y - \left(\rho_{\text{part}} - \rho_{\text{fluid}}\right) \\ \cdot V_{\text{part}} \cdot g \cdot \cos(\omega t) \end{bmatrix} \\
S &= \pi \cdot R_{\text{part}}^2 \\
C_d &\approx \frac{24}{\text{Re}} + \frac{6.0}{1.0 + \sqrt{\text{Re}}} + 0.4
\end{aligned}
\tag{1}
$$

where ($\rho_{\text{sphere}} - \rho_{\text{fluid}}$) is the difference between the density of the microcapsule and surrounding fluid, Re is the Reynolds number, $V_{\text{part}}$ is the microcarrier volume, $C_d$ is the drag coefficient at $\text{Re} < 2 \times 10^5$, $p$ is the stagnation pressure, $S$ is the microcapsule planar surface area, and $Z$ is the axis of rotation. The solution to these equations has been described in detail previously.[21] Briefly, a numerical solution to these equations was obtained by way of fourth order Runga Kutta integration scheme run on a local workstation, using an adaptive stepwise control algorithm to ensure convergence through the integration period and assuming a specific starting position ($x,y$) within the bioreactor. Using this numerical model, we have identified scaffold parameters (e.g., density and drag coefficient) that yield particle trajectories without any confounding wall collisions. Scaffolds were then fabricated from component microcarriers that meet these design criteria.

To compare resulting scaffold motion in the rotating bioreactor relative to the culture medium, we used a particle tracking system built for the rotating bioreactor as described previously.[21] In brief, the system is composed of a rotating CCD camera (Cohu, Inc., San Diego, CA) that is in synchrony with a rotating high aspect ratio vessel (HARV). Particle motions are videotaped (Sony SVO-9500 MD, Japan) and digitally re-recorded using a Sony Frame Code Generator and frame grabber (Media Cybernetics, Silver Spring, MD). Image analysis is performed using Image Pro (Phase 3 Imaging, Inc., Glenn Mills, PA). Lighter-than-water PLAGA microcarriers and microcarrier scaffolds were incubated in distilled water at room temperature for 24 h in a nonrotating bioreactor vessel, and their trajectories recorded during bioreactor rotation using the tracking apparatus. A temporal description of scaffold trajectory was measured over consecutive frames from which particle velocities were computed. From these velocity measurements and based on the geometry of the scaffolds (and diameter of isolated microcarriers), maximum fluid shear stress is estimated by assuming uniform flow past a single microcarrier and using the Stokes equation:

$$\sigma = \frac{-3 \quad \mu U}{2a} \tag{2}$$

where $\sigma$ is shear stress, $\mu$ is viscosity, $U$ is flow velocity, and $a$ is the diameter of the microcarrier.

## Cell seeding and culture

We used the human SaOS-2 line (ATCC no. HTB-85) which exhibits homogeneous and reproducible expression of cellular alkaline phosphatase over an infinite lifespan. For all experiments, cells were maintained in M199 (GIBCO BRL, Grand Island, NY) culture

medium supplemented with 10% fetal bovine serum (Sigma, St. Louis, MO), and 2.5 m*M* L-glutamine and 3 m*M* *b*-glycerol phosphate. SaOS-2 cells were grown to confluency and digested in 0.01% trypsin in 0.04% EDTA (GIBCO) for 10 min. Cells were then resuspended in a minimal amount of media, their numbers determined with a Coulter Counter (Beckman Coulter, Inc., Fullerton, CA), and diluted to an appropriate cell density. Before cell seeding, PLAGA scaffolds ($n = 36$) were washed in phosphate buffered saline (PBS), and placed inside a single bioreactor vessel (Synthecon, Houston, TX) filled with 55 mL of complete medium containing no cells. After 10 min, the bioreactor vessel was inoculated with $8 \times 10^6$ cells and mounted onto a multi-HARV rotating unit[21] turning at 25 rpm. Cell attachment to microcarrier scaffolds in the rotating vessel was estimated from the decrease of cell density in the supernatant fluid observed over 24 h. At time intervals of 4, 8, and 12 h, 0.5 mL of the cell suspension was removed from the bioreactor, resuspended in trypsin solution to dissociate cell aggregates, and cell numbers were determined using a Coulter counter. At 24 h, the entire cell suspension was removed and the cell number determined.

## Cell counting

Immediately after the seeding of the cells for an experiment, a random sampling ($n = 6–10$) of selected scaffolds was removed to determine the initial number of attached cells by means of a fluorometric DNA assay.[32] The remaining scaffolds were washed with PBS and divided equally into two experimental groups. Each group of scaffolds was placed respectively into two new bioreactor vessels and refed with 55 mL of fresh culture medium. To determine the effect of culture vessel rotation on cell function, one vessel was mounted onto a multi-HARV unit and rotated at 25 rpm and the other was cultured statically (no-rotation) as a control. Each vessel was cultured at 37°C and 5% $CO_2$ for 7 days. At days 3 and 7, additional scaffolds were removed for DNA quantification. Scaffolds used for DNA analysis were washed three times in PBS, combined with 3 mL of additional PBS containing 2 m*M* EDTA, and pulverized using a tissue homogenizer (PowerGen 35; Fisher, Pittsburgh, PA) with a 10-mm diameter saw-tooth generator for 1 min. Cells were ruptured by 2 min of further homogenization at 30,000 rpm with a 5-mm diameter flat-bottom generator. Homogenates were frozen at –70°C until the day of analysis. On the day of analysis, 1 mL of scaffold homogenate was combined with 7 μL of a 200-μg/mL solution of bisbenzimide H33258 dye (Calbiochem, San Diego, CA) and vortexed vigorously. Fluorescence was read using a Tecan Spectrafluor microplate reader (Tecan, Austria) with an emission wavelength of 465 nm and an excitation wavelength of 360 nm. Cell standards were used to convert measured fluorescence to cell numbers, and unseeded but cultured scaffolds were analyzed to determine any effect of PLAGA autofluorescence.

## Alkaline phosphatase (ALP) activity

ALP activity was measured by using adaptations of standard histochemical[33] and colorimetric[8] methods. At days 3 and 7, scaffolds were removed from both the rotating and nonrotating bioreactor vessels and washed two times with PBS. Scaffolds were then incubated for 30 min at 37°C with Napthol AS-BI (N-2250; Sigma) phosphate salt (0.5 mg/mL; Sigma) and *N,N*-dimethyl formamide (10 μL/mL, D-8654; Sigma) in 50 m*M* Tris buffer (pH 9.0), in the presence of Fast Red (Sigma, F-2768) violet salt (1.0 mg/mL). After 30 min, cells were washed two times with PBS and fixed by incubation in 2% paraformaldehyde for 30 min at 4°C. ALP staining was viewed by light microscopy. Scaffolds were fractured into halves to visualize cells in the interior regions of the 3-D structure.

In addition, ALP expression was quantified in each of the cell-scaffold homogenates used for fluorometric DNA analysis. Briefly, aliquots of cell homogenates were incubated at

37°C for 30 min in 0.1*M* $Na_2CO_3$ buffer solution (pH 10) containing 2m*M* $MgCl_2$ with disodium *p*-nitrophenyl phosphate (*p*NP-$PO_4$) as the substrate. Standard solutions were prepared by serial dilutions of 0.5 m*M* *p*-nitrophenol (*p*NP) in $Na_2CO_3$ buffer. Enzymatic activity was expressed as total nanometers of *p*NP produced per minute per total cell number determined by fluorometric DNA analysis. Absorbance was measured at 415 nm using a Tecan Spectrofluor microplate reader.

### Alizarin red calcium quantification

The effectiveness of sodium 1,2-dihydroxyanthraquinone-3-sulfonate, commonly known as alizarin red (ALZ), as a chelating compound and colorimetric reagent for spectrophotometric determination of calcium is well established.[34] We have adapted ALZ spectrophotometric methods for the determination of mineralized matrix production[35] on lighter-than-water PLAGA by osteoblast-like cells. Briefly, scaffolds were removed from the bioreactor, washed in $ddH_2O$, and incubated in 40 m*M* ALZ solution (pH 4.2) for 10 min at room temperature. To remove unreacted ALZ, scaffolds were washed 5–10 times in $ddH_2O$ (until water was clear). Scaffolds were then incubated in 10% cetyl pyridinium chloride for 15 min to solubilize reacted ALZ and pulverized using a tissue homogenizer (PowerGen 35; Fisher) with a 10-mm diameter saw-tooth generator. Serial dilutions of 1*N* $CaCl_2$ were used as standards. ALZ concentration per cell was calculated as molar equivalent $CaCl_2$ divided by the average cell number at each time point as determined by fluorometric DNA analysis. Absorbance was measured at 570 nm using a Tecan Spectrofluor microplate reader.

### SEM

Before seeding with cells, microcarriers and microcarrier scaffolds were coated with gold and visualized using a low field emission electron microscope (JEOL 6300) at 2 keV accelerating voltage. To evaluate cell attachment and morphology to lighter-than-water scaffolds cultured in the bioreactor, scaffolds were cultured as described above and removed at day 7 for SEM analysis. Attached cells were fixed to scaffold substrates by washing thoroughly with PBS, then incubation in 1% and 3% glutaraldehyde for 1 h and 24 h, respectively. After fixation, cells were washed with PBS, placed through a series of graded ethanol dehydrations, and allowed to air dry. Finally, cell scaffolds were coated with carbon and analyzed at 2 keV.

### Statistical analysis

Statistical analysis was performed using JMP IN 3.2.1 software (JMP IN®; SAS Institute, Inc., Belmont, CA). One-way analysis of variance was performed to determine any statistically significant relationship between the rotating and non-rotating conditions with respect to the quantity of reacted ALZ, ALP expression, and cell number. Statistical significance was attained at $p < 0.05$. Three scaffolds were analyzed at each time point and for each quantitative assay. Error bars indicate the standard deviation of the mean value.

## RESULTS

### Buoyant microcarrier fabrication

A typical lighter-than-water PLAGA microcarrier is shown in Figure 1(A). To demonstrate that we have successfully fabricated hollow microcarriers, some carriers were fractured after immersion in liquid nitrogen. A representative image is shown in Figure 1(B). The carriers were buoyant after immersion in deionized water, phosphate buffer solution, and tissue culture medium. Microcarriers were fabricated to produce lighter-than-water densities from 0.6 to 0.99 g/mL as estimated using of a density gradient column (ASTM D-1505). The

characteristic distribution of microcarrier sizes is represented in Figure 2. The majority of lighter-than-water microcarriers (47%) are within the range of 500 to 860 μm in diameter, with 19% from 300–500 μm, 8% at 100–300 μm, and 2% less than 100 μm. Though 29% of microcarriers were greater than 860 mm in diameter, only microcarriers 860 μm and below were used for scaffold fabrication.

## Scaffold fabrication and characterization

We have utilized the hollow microcarriers for the fabrication of 4 × 2.5 mm cylindrical scaffolds. By sintering at 60°C, amorphous polymer chains of adjacent microcarriers move past one another and interlock, forming a mechanical bond. Because this temperature is well below the melting temperature, we avoid collapse of individual microcarriers, thereby preserving their hollow, spherical geometry and the lighter-than-water density of the aggregate structure. Porosity is a result of the imperfect packing of spherical microcarriers inside the mold, and thus geometry dictates that there are no isolated spaces (pores) within the structure and that the network of pores in the scaffold is fully interconnected. The effect of sintering on the connectivity of microspheres was evident from SEM images showing two or more microspheres fused together at the contact regions [Fig. 3(A)]. Assuming the spheres approach a close packed configuration in the mold, the diameter of the scaffold pores can be represented as interstitial voids in the structure. Again, geometry dictates that the pore of the structure is given by $0.225R$ in the case of a tetrahedral site (a void surrounded by four spheres in the shape of regular tetrahedron) or $0.414R$ in an octahedral site (a void surrounded by six spheres in the shape of an octagon), where $R$ is the radius of the surrounding spheres. Microcarriers in the size range of 500–860 μm were used most frequently for scaffold fabrication, because they form structures with an expected pore size range of 113 to 356 μm shown to be suitable for osteoblast adherence and migration.[13,16] The porosity and pore size distribution of typical microcarrier scaffolds were measured using mercury porosimetry. Although the broad distribution of microcarrier size likely decreases the resulting pore diameter and increases packing efficiency, the measured porosity of 31% slightly exceeds that of close packing (26%). Figure 3(B) illustrates the average pore size distribution of 12 microcarrier scaffolds where the median pore of 187 μm is well within the theoretical expectation for close-packed spheres. Although the value median pore diameter exceeds the minimum requirement for cell ingrowth and migration,[12–14,16] the level of total pore volume or porosity of microcarrier scaffolds is 50–60% less than that of similar polymeric matrices proposed for bone repair.[12–14]

## Numerical model simulation and particle motion analysis

In a previous study, we solved the governing equations for microcarrier motion through the culture medium during bioreactor rotation and established that the path of lighter-than-water microcarriers would follow two characteristic motions with respect to the rotating medium. The first is a periodic circular motion, which at steady state had a velocity equal to the sedimentation velocity, and the second is a radial motion of the particle that reflected the drift of the particle toward the center of the bioreactor vessel. Figure 4(A) illustrates a model simulation of the motion of a single microcarrier with a density of 0.65 g/mL and 300-μm radius rotated at 25 rpm. From a starting position 10 mm from the bioreactor wall, the model predicts a radius of periodic motion of 21 mm, an instantaneous velocity of about 29 mm/s, and a centrifugal drift toward the center of the vessel. Figure 4(C) depicts the trajectory of a single microcarrier with identical physical parameters and bioreactor conditions input to the theoretical model (i.e., 0.65 g/mL an, 300 μm radius, and 25 rpm). An instantaneous velocity of 27 mm/s was calculated directly from microcarrier position data by dividing the distance traveled along the circular path by the elapsed time between frames. The primary and secondary motions exhibited by the microcarrier were nearly identical to motions

predicted by the theoretical model. These results guided us in the construction of 3-D scaffolds that are specifically designed to avoid scaffold collision with the outer wall.

Microcarrier scaffolds were constructed primarily from 500–860-μm lighter-than-water microcarriers and fashioned into 4 × 2.5 mm cylindrical discs. A time-lapsed image of typical scaffold motion in the bioreactor is shown in Figure 4(D). Particle tracking analysis revealed an instantaneous velocity of 98 mm/s and a trajectory completely absent of wall collisions once equilibrium motion was reached. At present, our theoretical model assumes a uniformly spherical particle shape. Using this model, a spherical particle of identical density and cross-sectional diameter would have an instantaneous velocity of 161 mm/s. However, microcarrier scaffolds do not behave as uniform spheres as is required for our numerical model. In fact, the scaffolds are shaped as cylindrical discs, and therefore, their associated drag coefficient differs by a factor of 1.5. Using the corrected drag coefficient, the predicted value of scaffold instantaneous velocity is 126 mm/s. Theoretical and experimental values of single microcarrier and microcarrier scaffold velocity are compared in Figure 4(B). A closer agreement with theory is exhibited by single microcarrier motion, whereas instantaneous velocity of microcarrier scaffolds deviates from the theoretical prediction by approximately 23%.

## Dynamic cell seeding

Cell attachment to microcarrier scaffolds during rotating culture was estimated from cell concentration profiles taken at times 4, 8, 12, and 24 h after co-inoculation with lighter-than-water scaffolds. The decreased concentration of suspended cells during culture is assumed to reflect the attachment of these cells to the scaffolds. A representative result is shown in Figure 5(A) in which cell density in the bioreactor medium decreased about 60%. By dividing the estimated quantity of attached cells by the total number of scaffolds present in culture, we estimated cell seeding at approximately $1.4 \times 10^5$ cells/scaffold. After 24 h of dynamic seeding, a sampling of 6 to 10 cell scaffolds was used to measure directly the number of cells attached to scaffolds using fluorometric DNA analysis. Measurements of attached cells were in excellent agreement with cell concentration estimates with an average value of $1.3 \times 10^5$ cells per scaffold and standard deviation of $2.0 \times 10^4$ cells. The average surface area per scaffold was calculated to be approximately 2 $cm^2$, resulting in a cell seeding density of approximately $6.5 \times 10^4$ cells/$cm^2$.

## Cell growth and penetration

Cell proliferation was examined on lighter-than-water microcarrier scaffolds over a period of 7 days with cell numbers measured immediately after cell seeding and at days 3 and 7 [Fig. 5(B)]. Cells cultured on lighter-than-water scaffolds in the rotating bioreactor show evidence of a lower rate and extent of proliferation than those cultured on nonrotating controls. Significant differences in cell numbers could be detected by day 7 ($p < 0.05$). Using SEM, we verified the presence of cells within the pores of the scaffold that nearly cover the entire surface of the internal microcarriers [Fig. 5(C,D)]. By progressively focusing the microscope down the pore of the structure, we estimate that cells have penetrated as deep as 800 μm.

## Cell phenotypic expression

The retention of osteoblastic phenotype was evaluated by ALP histochemical staining and colorimetric analysis. Cells were stained for ALP expression on lighter-than-water scaffolds in the rotating bioreactor and on the nonrotating 3-D controls at days 3 and 7 [Fig. 6(A–D)]. Positive ALP staining is evident at each time point and for each culture condition. At each time point, more cells per unit area are present on scaffolds cultured under nonrotating 3-D conditions [Fig. 6(B,D)] than those cultured in the rotating bioreactor [Fig. 6 (A,C)], which

is consistent with the fluorometric DNA analysis described above. In addition, color-imetric analysis was also performed at 24 h and at day 7. These results were normalized by the actual number of cells present in each scaffold. Figure 7(A) gives a graphical illustration that by day 7 the actual amount of ALP expressed per cell is significantly higher for cells cultured in the rotating bioreactor than on non-rotating 3-D controls ($p < 0.05$).

The production of calcified matrix was analyzed by ALZ histochemical staining. In Figure 6(E,F), scaffolds cultured in the rotating bioreactor showed substantially greater alizarin-positive extracellular matrix material by day 7 as compared with 3-D controls ($p < 0.05$). To quantify the amount of early-stage calcified matrix formation, we have adapted ALZ staining techniques for colorimetric analysis by solubilizing the red matrix precipitate with cetyl pyridinium chloride to yield a purple solution suitable for optical density measurements at 562 nm. Quantities of ALZ-stained matrix were expressed as a molar equivalent $CaCl_2$ concentration and normalized by the average number of cells per scaffold as determined in companion proliferation studies. Figure 7(B) reveals significant increases in the quantity of ALZ-stained matrix produced on lighter-than-water scaffolds under rotating conditions at days 3 and 7 as compared with nonrotating controls.

## DISCUSSION

In this study, we have presented a novel method for the fabrication of hollow, lighter-than-water PLAGA microcarriers specifically designed for cell culture in the HARV rotating bioreactor. Using theoretical simulation and particle tracking methods, we have thoroughly described the velocity and characteristic motions of these particles during bioreactor rotation. Using our theoretical model,[21] we have found that lighter-than-water microcarriers rapidly reach a terminal velocity in the fluid medium as bioreactor rotation is initiated. In addition, microcarriers exhibit a primary periodic circular motion at a velocity equal to the microcarrier sedimentation velocity with respect to the rotating fluid as well as a secondary centrifugal drift toward the center of the bioreactor vessel. As a result, lighter-than-water PLAGA microcapsules are excellent cell microcarriers providing a low shear, nonturbulent flow environment for attached cells that avoids damaging collisions with the bioreactor wall. For the lighter-than-water PLAGA microcarriers considered in this study, particle motion and velocity were nearly identical to the observed results of companion particle image tracking experiments as seen in Figure 4(B). The agreement of the theoretical and experimental results should prove to be a very useful outcome in the further design and optimization of PLAGA microcarriers.

It has been shown by our lab[21] and others[19,22,36] that when osteoblast cells are co-inoculated with microcarriers in the rotating bioreactor, a random aggregation occurs generated by the adherence of cells to microcarrier beads and the formation of cellular bridges between adjacent microcarriers. However, the random aggregation that occurs in the rotating bioreactor is not conducive to strict quantitative comparison, because the size and shape of cell-bead aggregates as well as the degree of aggregation varies greatly. Such a limitation is overcome in our system by the sintered preassembly of microcarriers into dimensionally reproducible cell scaffolds before culture in the bioreactor. Furthermore, the microcarrier sintering method is not limited by the adverse effects associated with the particulate leaching, and consequently, no unwanted degradation of the scaffold occurred during fabrication.

We have successfully fabricated lighter-than-water polymer scaffolds using sintered microcarrier methods, which have a median pore size of 187 μm and a fully interconnected interior pore network. Using our particle tracking system, we are able to calculate the instantaneous velocity of microcarrier scaffold motion through the fluid medium. The

motion of the scaffold through the fluid creates an effective flow of culture medium past the cells at or near the surface of the scaffold. Using the instantaneous velocity determined in particle tracking experiments and assuming a uniform flow past a single component microcarrier, the maximum wall shear stress on cells at the surface of the microcarrier may be calculated using the Stokes Equation (2). On scaffolds composed of lighter-than-water microcarriers averaging 0.65 g/mL in density and 500 to 860 μm in diameter, we obtain maximum shear stress values of 2.7 to 4.7 dynes/$cm^2$. In contrast to motion analysis studies of single microcarriers, the instantaneous velocity of porous microcarrier scaffolds is significantly less than the theoretical model prediction for a uniform sphere of the same size and density. This result indicates a greater effective drag force for porous scaffolds, which is only partially explained by scaffold cylindrical shape and also may be attributed to a flow of fluid through the scaffold interacting with successive layers of fixed microcarriers. We speculate that osteoblast cells on and within the porous scaffold experience a shear stress less than that of single bead motion, because the aggregate scaffold structure has an effective particle radius much greater than a single bead. If in fact fluid flows to the interior regions of the scaffold, such a condition might serve to enhance mass transport of $O_2$ and nutrients, while also speeding waste and degradation product efflux. Using the methods of theoretical modeling and particle motion analysis described in this study and others, we have begun to investigate the fluid permeability of lighter-than-water 3-D scaffolds in an effort to establish unequivocally the existence of fluid flow throughout the porous structure

A high, spatially uniform distribution of attached cells has been shown to be highly significant for the formation of *in vitro* tissues from anchorage-dependant cells.[37,38] Conventional methods of cell seeding of 3-D scaffolds under static conditions often confines cell attachment and tissue growth at or near the initially seeded surface.[13] We believe that cell seeding in the rotating bioreactor is an attractive alternative to static seeding methods for these scaffolds, and may be used to enhance cell migration to the interior of the scaffold and promote homogeneity of initial cell seeding from one scaffold to another. However, a more thorough examination of the uniformity and distribution of dynamic cell attachment in the bioreactor must be performed.

The hydrodynamic flow environment produced by the motion lighter-than-water scaffolds in the rotating bioreactor is a likely enhancer of $O_2$ and nutrient transport to cells at the near surface (external) of the scaffold and possibly those in the scaffold interior (internal), which may act to advance phenotype development and tissue formation in our system. In contrast, a recent investigation by Goldstein et al.[14] examining primary rat osteoblast cultures on porous PLAGA foams in a rotating bioreactor, reported no statistically significant change in either cell density or differentiation after 7 days as compared with static 3-D controls. The authors concluded that hydrodynamic and mechanical forces in their model did not have a significant influence on cells cultured in the rotating bioreactor. It is possible that the flow conditions in the interior of the foam scaffolds are significantly different from those used in this study or the effect of wall collisions[39] on cells residing on the surface of the foams in the rotating bioreactor or both alter cell behavior sufficiently to account for this difference. In the case of the lighter-than-water scaffolds, collisions with other scaffolds and the wall of the bioreactor are significantly reduced or altogether eliminated. However, we have made no distinction between the behavior of cells cultured in the external and internal regions of our scaffolds in this study. We recognize that the hydrodynamic environment experienced by cells in the interior of the scaffold may be altogether different than that of cells near the surface, and as such, we hope to uncover any differential effects on cell function in future experiments.

With regards to scaffolds of 0.65 g/mL aggregate density and 500–860 μm composite microcarriers in the rotating bioreactor, we have shown that osteoblast-like cell proliferation

is not significantly increased as compared with nonrotating static controls. In fact, a significant decrease in cell number can be detected by day 7 of bioreactor culture. In contrast, the development of osteoblastic phenotype is enhanced in these cells, as determined by a significant elevation in ALP expression. This reciprocal relationship between cell growth and phenotype development is consistent with previous studies regarding the behavior of osteoblast cells.[40] In addition, Stein et al.[41–44] have shown that the onset of mineralized matrix production by osteoblasts proceeds through a maximum in ALP expression. In our study, we have shown that the increase in ALP expression by osteoblast cells cultured in the rotating bioreactor is accompanied by an elevation in early stage mineralized matrix production. However, Stein et al.[41,42] have also reported that the onset of mineralized matrix production begins at 14 days in culture, whereas we observed significant elevations in matrix production by cells cultured on lighter-than-water scaffolds in the rotating bioreactor by day 3. These results suggest that this system of culture may eventually be used to the rapid synthesis of *in vitro* mineralized tissues. However, it is important to note that the particular scaffolds considered herein present a unique hydrodynamic environment to attached cells. Moreover, this system of scaffold fabrication can generate a variety of microcarrier scaffolds of different component size ranges, associated 3-D architecture, and density. As these physical parameters are varied, the fluid dynamic forces and transport phenomena for attached cells may be altogether different. In such cases of altered scaffold geometry, the relationship among the hydrodynamic factors, cell density, cell proliferation, and cell differentiation is not yet known.

In conclusion, we have fabricated lighter-than-water porous 50:50 PLAGA scaffolds for culture in the high aspect ratio rotating bioreactor. These scaffolds adopt a particle trajectory absent of confounding wall collisions, while maintaining a 3-D geometry open to mass transport of nutrients and waste products. This model combines 3-dimensionality and fluid transport in the absence of damaging wall collisions and may be a closer approximation of the *in vivo* environment of the cell, thereby expanding our capacity for *ex vivo* tissue synthesis. Although additional studies using primary cells in culture and various scaffold porosities should be performed, this system shows promise as a novel method for developing bone graft quality tissue.

## Acknowledgments

The authors thank Dr. David Meaney for his assistance with the numerical modeling program, Dr. Jaspal Khillan for the use of his light microscope facility at the Wistar Institute, and Eric Johnston for technical support with image analysis. Dr. Laurencin is the recipient of a Presidential Faculty Fellowship Award from the National Science Foundation, and author Edward Botchwey is a Ph.D. fellow of the National Consortium for Graduate Degrees for Minorities in Engineering.

Contract grant sponsor: NASA; contract grant number: NAG9-832

Contract grant sponsor: NIH; contract grant number: AR07132-23

## References

1. Langer R, Vacanti JP. Tissue engineering. Science. 1993; 260(5110):920–926. [PubMed: 8493529]
2. Langer R, Vacanti JP, Vacanti C, Atala A, Freed LE, Vunjak-Novakovic G. Tissue engineering: Biomedical applications. Tissue Eng. 1995; 1(2):151–161. [PubMed: 19877924]
3. Burwell, RG. History of bone grafting and bone substitutes with special reference to osteogenic induction.. In: Urist, MR.; Burwell, RG., editors. Bone grafts, derivatives, and substitutes. Butterworth-Heinemann; Oxford: 1994. p. 3
4. Cook SD, Baffes GC, Wolfe MW, Sampath TK, Rueger DC, Whitecloud TS. The effect of recombinant human osteogenic protein-1 on healing of large segmental bone defects. J Bone Joint Surg Am. 1994; 76(6):827. [PubMed: 8200889]

5. Gazdag AR, Lane JM, Glaser D, Forster RA. Alternative to autogenous bone graft: Efficacy and indications. J Am Acad OrthoP Surg. 1995; 3(1):1. [PubMed: 10790647]
6. Casserbette M, Murray AB, Closs EI, Erfle V, Schmidt J. Bone-formation by osteoblast-like cells in a 3-dimensional cell-culture. Calcif Tissue Int. 1990; 46(1):46–56. [PubMed: 2295023]
7. Masi L, Franchi A, Santucci M, Danielli D, Arganini L, Giannone V, Formigli L, Benvenuti S, Tanini A, Beghe F, Mian M, Brandi ML. Adhesion, growth, and matrix production by osteoblasts on collagen substrata. Calcif Tissue Int. 1992; 51(3):202–212. [PubMed: 1330236]
8. Rattner A, Sabido O, Massoubre C, Rascle F, Frey J. Characterization of human osteoblastic cells: Influence of the culture conditions. In vitro Cell Dev Biol Anim. 1997; 33(10):757–762. [PubMed: 9466680]
9. Mizuno M, Shindo M, Kobayashi D, Tsuruga E, Amemiya A, Kuboki Y. Osteogenesis by bone marrow stromal cells maintained on type I collagen matrix gels *in vivo*. Bone. 1997; 20(2):101–107. [PubMed: 9028533]
10. Elghannam A, Ducheyne P, Shapiro IM. Bioactive material template for *in vitro* synthesis of bone. J Biomed Mater Res. 1995; 29(3):359–370. [PubMed: 7615587]
11. Ducheyne P, Elghannam A, Shapiro I. Effect of bioactive glass templates on osteoblast proliferation and *in vitro* synthesis of bone-like tissue. J Cell Biochem. 1994; 56(2):162–167. [PubMed: 7829574]
12. Ishaug SL, Crane GM, Miller MJ, Yasko AW, Yaszemski MJ, Mikos AG. Bone formation by three-dimensional stromal osteoblast culture in biodegradable polymer scaffolds. J Biomed Mater Res. 1997; 36(1):17–28. [PubMed: 9212385]
13. Ishaug-Riley SL, Crane-Kruger GM, Yaszemski MJ, Mikos AG. Three-dimensional culture of rat calvarial osteoblasts in porous biodegradable polymers. Biomaterials. 1998; 19(15):1405–1412. [PubMed: 9758040]
14. Goldstein AS, Guoming Z, Grayson E, Morris BS, Meszlenyi BS, Mikos AG. Effect of osteoblastic culture conditions on the structure of poly(d,l-lactic-*co*-glycolic acid) foam scaffolds. Tissue Eng. 1999; 5(5):421–433. [PubMed: 10586098]
15. Devin JE, Attawia MA, Laurencin CT. Three-dimensional de gradable porous polymer-ceramic matrices for use in bone repair. J Biomater Sci Polym Ed. 1996; 7(8):661–669. [PubMed: 8639475]
16. Laurencin CT, Attawia MA, Elgendy HE, Herbert KM. Tissue engineered bone-regeneration using degradable polymers: The formation of mineralized matrices. Bone. 1996; 19(1):S93–S99.
17. Thomson RC, Yaszemski MJ, Powers JM, Mikos AG. Hydroxyapatite fiber reinforced poly(alpha-hydroxy ester) foams for bone regeneration. Biomaterials. 1998; 19(21):1935–1943. [PubMed: 9863527]
18. Laurencin CT, ElAmin SF, Ibim SE, Willoughby DA, Attawia M, Allcock HR, Ambrosio AA. A highly porous 3-dimensional polyphosphazene polymer matrix for skeletal tissue regeneration. J Biomed Mater Res. 1996; 30(2):133–138. [PubMed: 9019476]
19. Granet C, Laroche N, Vico L, Alexandre C, Lafage-Proust MH. Rotating-wall vessels, promising bioreactors for osteoblastic cell culture: Comparison with other 3D conditions. Med Biol Eng Comput. 1998; 36(4):513–519. [PubMed: 10198539]
20. Klement BJ, Spooner BS. Utilization of microgravity bioreactors for differentiation of mammalian skeletal tissue. J Cell Biochem. 1993; 51(3):252–256. [PubMed: 8501126]
21. Pollack SR, Meaney DF, Levine EM, Litt M, Johnston ED. 3-D self assembled scaffolds in a rotating bioreactor. Tissue Eng. To appear.
22. Qiu Q, Ducheyne P, Gao H, Ayyaswamy P. Formation and differentiation of three-dimensional rat marrow stromal cell culture on microcarriers in a rotating-wall vessel. Tissue Eng. 1998; 4(1):19–34. [PubMed: 11541090]
23. Lewis ML, Moriarity DM, Campbell PS. Use of microgravity bioreactors for development of an *in vitro* rat salivary-gland cell-culture model. J Cell Biochem. 1993; 51(3):265–273. [PubMed: 8501128]
24. Becker JL, Prewett TL, Spaulding GF, Goodwin TJ. 3-Dimensional growth and differentiation of ovarian tumor-cell line in high aspect rotating-wall vessel: Morphologic and embryologic considerations. J Cell Biochem. 1993; 51(3):283–289. [PubMed: 8501130]

25. Prewettt TL, Goodwin TJ, Spaulding GF. Three-dimensional modeling of t-24 human bladder carcinoma cell line: A new simulated microgravity culture vessel. J Tissue Cult Methods. 1993; 15:29–36.
26. Watts PJ, Davies MC, Melia CD. Microencapsulation using emulsification solvent evaporation: An overview of techniques and applications. Crit Rev Ther Drug Carrier Syst. 1990; 7(3):235–259. [PubMed: 2073688]
27. Jalil R, Nixon R. Microencapsulation using poly(d,l-lactic acid). II. Effect of polymer molecular-weight on the microcapsule properties. J Microencapsul. 1990; 7(2):245–254. [PubMed: 2329449]
28. Iwata M, McGinity JW. Preparation of multiphase micro-spheres of poly(d,l-lactic acid) and poly(d,l-lactic-*co*-glycolic acid) containing a W/O emulsion by a multiple emulsion solvent evaporation technique. J Microencapsul. 1992; 9(2):201–214. [PubMed: 1593404]
29. Hausberger AG, Deluca PP. Characterization of biodegradable poly(d,l-lactide-*co*-glycolide) polymers and microspheres. J Pharm Biomed Anal. 1995; 13(6):747–760. [PubMed: 7669829]
30. Crotts G, Park TG. Preparation of porous and nonporous bio-degradable polymeric hollow microspheres. J Controlled Release. 1995; 35(2–3):91–105.
31. Arshady R. Preparation of biodegradable microspheres and microcapsules. II. Polyactides and related polyesters. J Controlled Release. 1991; 17(1):1–21.
32. Labarca C, Paigen K. A simple, rapid and sensitive DNA assay procedure. Anal Biochem. 1980; 102:344–352. [PubMed: 6158890]
33. Van Belle H. Kinetics and inhibition of alkaline phosphatases from canine tissues. Biochim Biophys Acta. 1972; 289:158–168. [PubMed: 4564052]
34. Wu L, Forsling W. Potentiometric and spectrophotometric study of calcium and alizarin red S complexation. Acta Chem Scand. 1992; 46:418–422.
35. Stanford CM, Jacobson PA, Eanes ED, Lembke LA, Midura RJ. Rapidly forming apatitic mineral in an osteoblastic cell line. J Biol Chem. 1995; 270:9420–9428. [PubMed: 7721867]
36. Qiu QQ, Ducheyne P, Ayyaswamy PS. Fabrication, characterization, and evaluation of bioceramic hollow microspheres used as microcarriers for 3-D bone tissue formation in rotating bioreactors. Biomaterials. 1999; 20(11):989–1001. [PubMed: 10378799]
37. Freed LE, Vunjak-Novakovic G. Culture of organized cell communities. Adv Drug Delivery Rev. 1998; 33(1–2):15–30.
38. Vunjak-Novakovic G, Obradovic B, Martin I, Bursac PM, Langer R, Freed LE. Dynamic cell seeding of polymer scaffolds for cartilage tissue engineering. Biotechnol Prog. 1998; 14(2):193–202. [PubMed: 9548769]
39. Cherry RS, Papoutsakis ET. Physical-mechanisms of cell-damage in microcarrier cell-culture bioreactors. Biotechnol Bioeng. 1988; 32(8):1001–1014. [PubMed: 18587818]
40. Owen TA, Aronow M, Shalhoub V, Barone LM, Wilming L, Tassinari MS, Kennedy MB, Pockwinse S, Lian JB, Stein GS. Progressive development of the rat osteoblast phenotype *in vitro:* Reciprocal relationships in expression of genes associated with osteoblast proliferation and differentiation during formation of the bone extracellular matrix. J Cell Physiol. 1990; 143:420–430. [PubMed: 1694181]
41. Lian, J.; Stein, GS. Mechanisms regulating osteoblast proliferation and differentiation.. In: Bilezikian, JP.; Raisz, LG.; Rodan, GA., editors. Principles of bone biology. Academic Press; San Diego: 1996. p. 69-86.
42. Stein GS, Lian JB, Stein JL, Van Wijnen AJ, Montecino M. Transcriptional control of osteoblast growth and differentiation. Physiol Rev. 1996; 76:593–629. [PubMed: 8618964]
43. Stein GS, Lian JB, Owen TA. Relationship of cell growth to the regulation of tissue-specific gene expression during osteoblast differentiation. FASEB J. 1990; 4:3111–3123. [PubMed: 2210157]
44. Stein GS, Lian JB, Gerstenfeld LG, Shalhoub V, Aronow M, Owen T, Markose E. The onset and progression of osteoblast differentiation is functionally related to cellular proliferation. Connect Tissue Res. 1989; 20:3–13. [PubMed: 2612161]

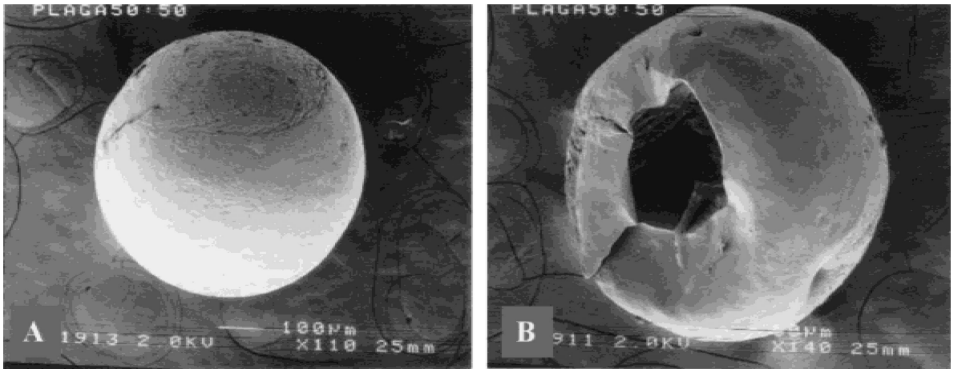


**Figure 1.**
SEM micrograph of hollow microcarrier morphology. (A) An intact hollow microcapsule of PLAGA 50:50 (original magnification x110). (B) Hollow internal morphology is confirmed by visualization after immersion and fracture in liquid $N_2$ (original magnification x140).

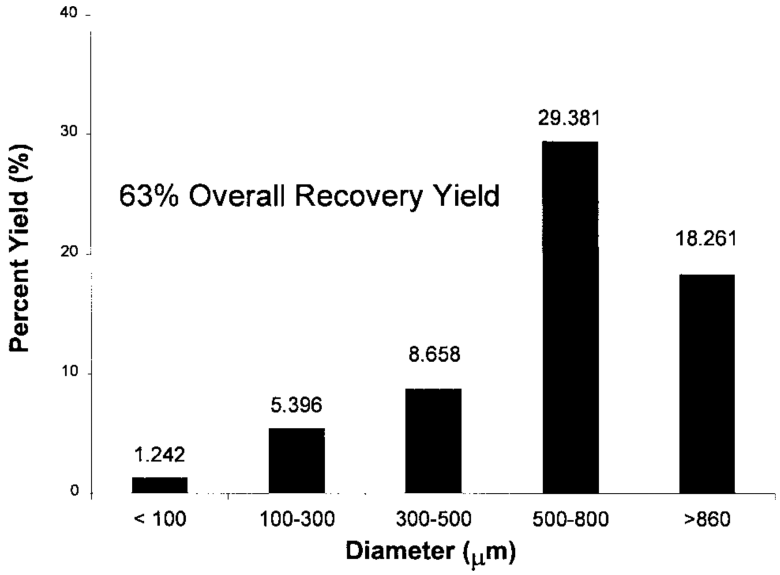


**Figure 2.**
Size distribution and percent yield of hollow microcarriers. Yield is defined as the fraction of starting raw material (PLAGA) that is recovered in the form of lighter than-water microcarriers after fabrication.

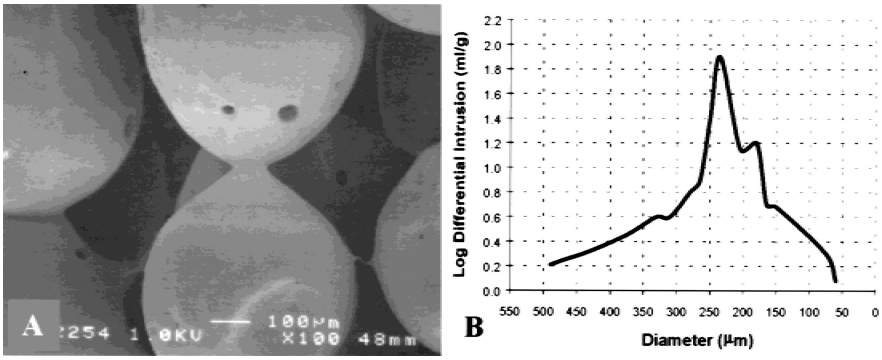


**Figure 3.**

Characterization of lighter-than-water scaffolds by SEM and mercury porosimetry. (A) SEM micrograph of polymer scaffold formed by the sintered microsphere method, using spheres with diameters between 500–860 μm. The sintered microspheres created an interconnected, porous structure suitable for cellular proliferation and tissue ingrowth (original magnification x100). (B) A plot log differential mercury intrusion versus pore diameter illustrates typical pore size distribution of lighter-than-water composed of 500–860-μm hollow microcarriers.

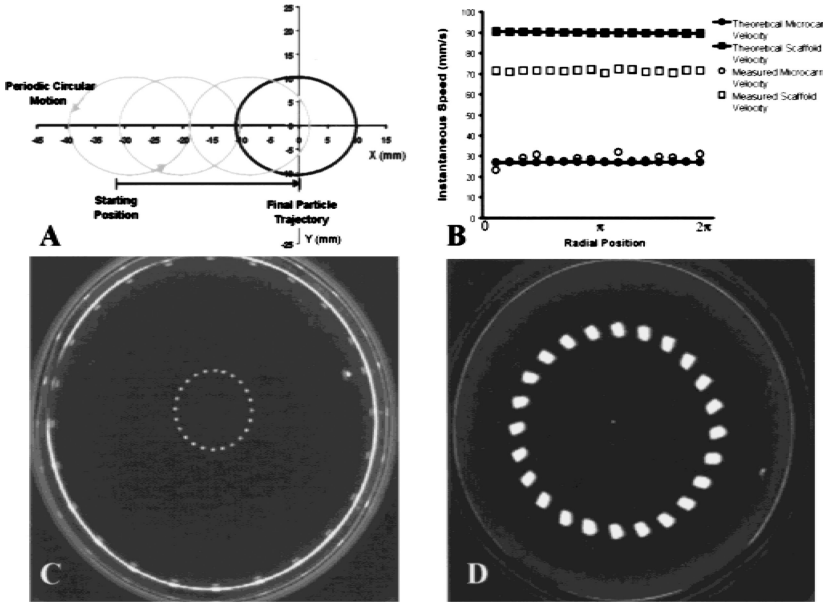


**Figure 4.**

Lighter-than-water microcarrier and scaffold motion in the HARV rotating bioreactor. (A) Theoretical prediction of the trajectory for a 600-μm hollow PLAGA microcarrier in the rotating bioreactor at 25 rpm (density 0.65 g/mL). (B) Comparison of a single microcarrier and a single scaffold instantaneous speed. Single microcarrier data for a 600-μm particle with density 0.65 g/mL is in good agreement with theory. Microcarrier scaffold data for a 4 × 2.5 mm, 0.65 g/mL scaffold deviates significantly from the theoretical prediction for a uniform sphere of similar size and density. (C) Trajectory of a 600-μm hollow PLAGA microcarrier in the rotating bioreactor turning at 25 rpm. Consecutive frames were recorded and digitized to render a temporal description microcarrier motion. The diameter of the surrounding vessel wall is approximately 100 mm. (D) Trajectory of a 4 × 2.5 mm scaffold in the rotating bioreactor turning at 25 rpm. The scaffold is composed of 500–860-μm hollow PLAGA microcarriers and has an aggregate density of 0.65 g/mL.

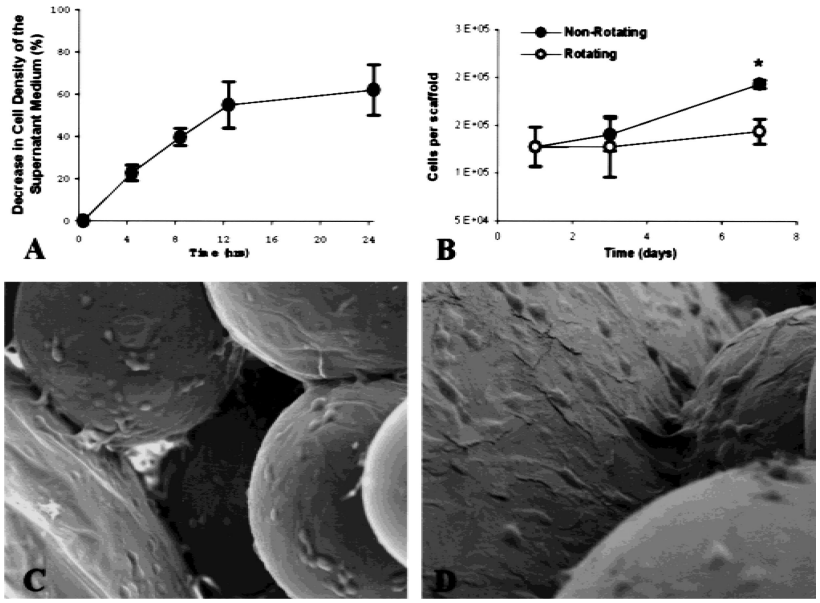


**Figure 5.**

Analysis of cell attachment and growth during bioreactor rotation. (A) Cell concentration decreased by 60% on average after 24 h of co-inoculation with lighter-than-water scaffolds in the rotating bioreactor, and initial cell attachment was calculated accordingly. (B) DNA cell counting to confirm initial cell seeding was in good agreement with estimates determined from cell concentration. Significantly, fewer cells were detected on lighter-than-water scaffolds cultured in a rotating bioreactor (25 rpm) by 7 days were by day as compared with nonrotated 3-D controls (asterisk denotes significance obtained at 5% type I error and $n = 3$). (C,D) SEM micrographs (original magnification x150 and x300, respectively) of sintered microsphere scaffold cultured with SaOS osteoblasts cells for 7 days. The cells were found on and between the microspheres. The cells bridged the microspheres and had completely covered the spheres. Cell extensions were found throughout the structure.

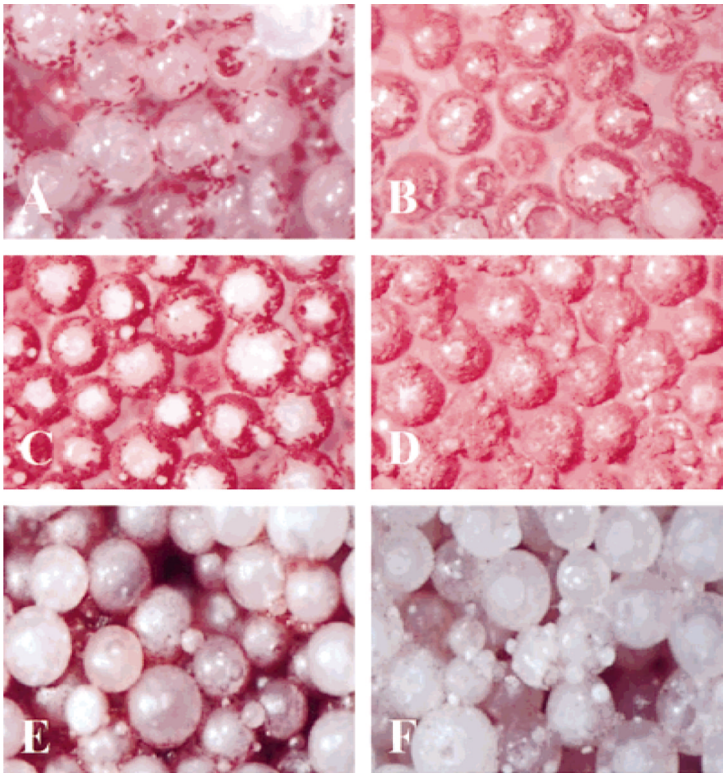


**Figure 6.**
Light micrographs (original magnification x50) showing phenotypic expression and early mineralized matrix synthesis by osteoblast-like cells in the rotating bioreactor. (A–D) Alkaline phosphatase expression by osteoblast-like cells cultured under rotating conditions at days 3 (A) and 7 (C). Right panels show companion micrographs of alkaline phosphatase expression on nonrotated 3-D controls at days 3 (B) and 7 (D). (E–F) Lighter-than-water scaffolds were cultured in the bioreactor for 7 days under static conditions (E) and 25 rpm rotation (F). Samples were stained with ALZ to detect mineralized extracellular matrix. Substantially more alizarin-positive material was observable on 3-D scaffolds cultured under rotating conditions.

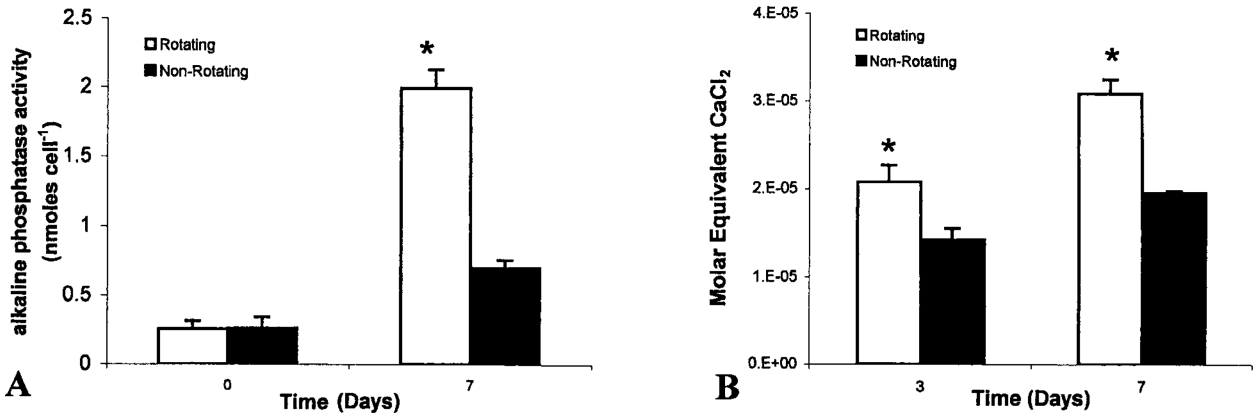


**Figure 7.**

Colorimetric determination of alkaline phosphatase expression and mineralized matrix synthesis. (A) Aliquots of individual scaffold homogenate were diluted to a known concentration and analyzed for alkaline phosphatase expression. Optical density measurements were determined at 415 nm. Quantities of alkaline phosphatase were normalized by dividing the measured quantity by the total number of cells present on the scaffold from which the homogenate was prepared. (B) To quantify the amount of ALZ that reacts with mineralized matrix, we adapted a technique that solubilizes the red matrix precipitate with cetyl pyridinium chloride to yield a purple solution suitable for optical density measurements at 562 nm. The concentration of $Ca^{2+}$ equivalents in scaffold homogenate was determined by using a $CaCl_2$ standard. For each time point, molar equivalent quantities were normalized for the average number of cells per scaffold as determined by companion fluorometric DNA analysis.